Muon Neutrino Disappearance – Sensitivity Analysis

Gabriel Varela

July 6, 2018

Introduction

The neutrinos shown in the typical Standard Model table of elementary particles – the electron, muon and tau neutrinos (ν_e, ν_μ, ν_τ) – are eigenstates of the weak force, created in charged current interactions between a W^+ boson, a neutrino and the associated charged anti-lepton (e^+ for the ν_e, μ^+ for the ν_μ and τ^+ for the ν_τ).

But these weak eigenstate neutrinos are not themselves eigenstates of the free-particle Hamiltonian. These mass eigenstates (ν_1, ν_2, ν_3) are linear combinations of the weak eigenstate neutrinos, related by

$$|\nu_\alpha\rangle = \sum_i U^\star_{\alpha,i} |\nu_i\rangle$$

where $\alpha \in \{e, \mu, \tau\}$ and $i \in \{1, 2, 3\}$.

Thus, a weak eigenstate neutrino created in an interaction (itself a superposition of mass eigenstates) will oscillate between different superpositions of these mass eigenstates as they travel freely:

$$|\nu_\alpha\rangle \to e^{-iHt/\hbar} |\nu_\alpha\rangle = \sum_i U^\star_{\alpha,i} |\nu_i\rangle \, e^{-im_i^2 L/E}$$

where we let $c, \hbar = 1$ and used the ultrarelativistic limit ($p_i << m_i$) to write $t \approx L$, the distance travelled, and $E_i = E + \frac{m_i^2}{2E}$, where E is the energy of the ν_α. Thus,

$$\begin{aligned} P_{\alpha\to\beta} &= |\, \langle\nu_\beta|\, e^{-iHt/\hbar} \,|\nu_\alpha\rangle \,|^2 \\ &= \big|\big(\sum_j \langle\nu_j|\, U_{\beta,j}\big)\big(\sum_i U^\star_{\alpha,i} e^{-im_i^2 L/E} \,|\nu_i\rangle\,\big)\big|^2 \\ &= \big|\sum_i U_{\beta,j} U^\star_{\alpha,i} e^{-im_i^2 L/E}\big|^2 \end{aligned}$$

U has three independent degrees of freedom, usually written as angles $\theta_{1,2}$, $\theta_{2,3}$ and $\theta_{1,3}$. With the experimentally discerned values for the matrix elements, $U_{\alpha,i}$, and the mass differences $\Delta m^2_{i,j}$ (of the order $\Delta m^2_{1,2} \approx 10^{-3}$ eV and $\Delta m^2_{2,3} \approx 10^{-5}$ eV) this relation gives us the oscillations shown in Figure 1.

Recent experiments, however, have shown some anomalies in the low L/E regime, where the traditional 3-neutrino oscillation theory predicts no oscillation should exist. In particular, the LSND experiment in Los Alamos in 1993-8 reported an excess of $\bar{\nu_e}$ from a beam of $\bar{\nu_\mu}$ at $L \approx 30m$. These low E/L oscillations are consistent with a theory that includes a fourth 'sterile' mass eigenstate neutrino, ν_4, that doesn't interact but affects oscillations, with a mass splitting $\Delta m^2_{1,4} \approx 1$ eV. This leads to an effective probability

$$P_{\alpha\to\beta} = \sin^2(2\theta_{4,1}) \sin^2\left(1.27 \frac{\Delta m_{4,1} L}{E}\right)$$

when $\Delta m^2_{4,1}$ is written in eV, L in km and E in GeV.

The Short-Baseline Neutrino experiment at Fermilab sets out to test this with three detectors in the line of the booster neutrino beam, all at distances of less than 1km from the beam target. This note looks at determining the sensitivity of the experiment in the $(\sin^2 2\theta, \Delta m^2)$ phase space, in models of varying intensity, as well as looking at the effect exposure and resolution have on this sensitivity.

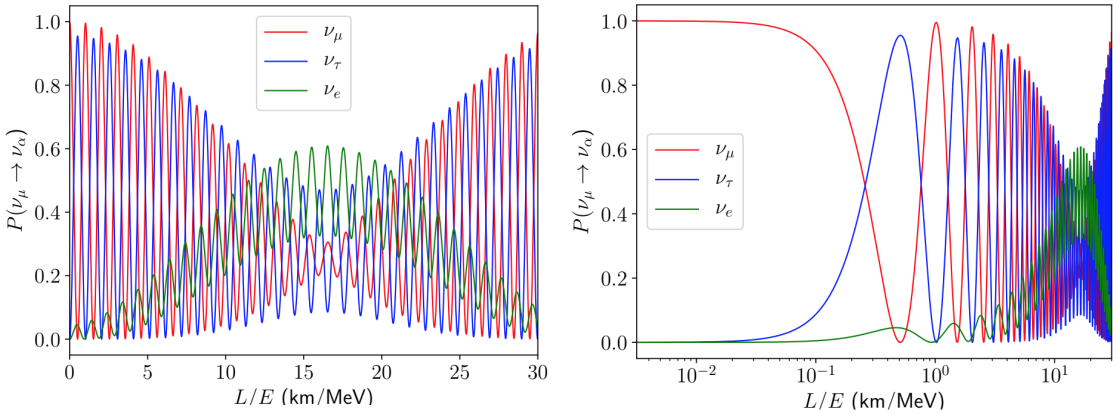

Figure 1: Muon neutrino disappearance for a beam initially composed only of ν_μ. The right panel shows a logarithmic x-axis, where we see that at low L/E there should be no oscillations if this model proves correct.

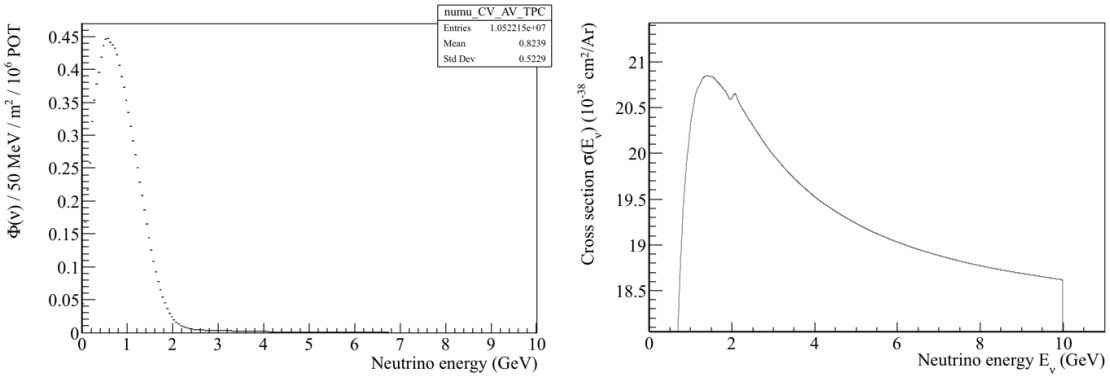

Figure 2: Left: The flux 470m from the source in the null case. Right: The cross-section for neutrino interactions in argon.

Base Case

We are given a file with the information on the flux at a distance of 470m from the target and on the cross-section for muon neutrino interactions in Argon (see Figure 2). Using these we can extract predictions for the 'base case' of a single detector 600m from the target (ICARUS) assuming perfect knowledge of the flux.

Given an exposure of 6×10^{20} POT (protons on target), we first normalise the units of the given flux and cross-section (ϕ' and σ') as

$$\phi_i = \phi_i' \times \frac{6 \times 10^{20} \text{ POT}}{10^6}$$
$$\sigma_i = \sigma_i' \times 10^{-42} \text{ m}^3 \times n_{Ar}$$

where the number of argon atoms in the detector is calculated as $n_{Ar} = V_{active} \times \rho_{LAr}/A_{Ar}$, where A_{Ar} is the atomic mass of argon. (The subscripts refer to the energy bins. The cross-section was linearly interpolated in order to make it comparable to the flux.)

If this flux is the true flux at 470m in the null case of no oscillations, we obtain the null prediction by adjusting for the $1/r^2$ fall in intensity and multiplying the flux and cross-section and the oscillation prediction by factoring in the probability of oscillation *away* from muon neutrinos:

$$N_i^{null} = \phi_i \times \frac{470 \text{ m}}{600 \text{ m}} \times \sigma_i$$
$$N_i^{osc} = N_i^{null} \times \left\{1 - \sin^2(2\theta) \sin^2\left(1.27 \frac{\Delta m^2 \times 0.6}{E_i}\right)\right\}$$

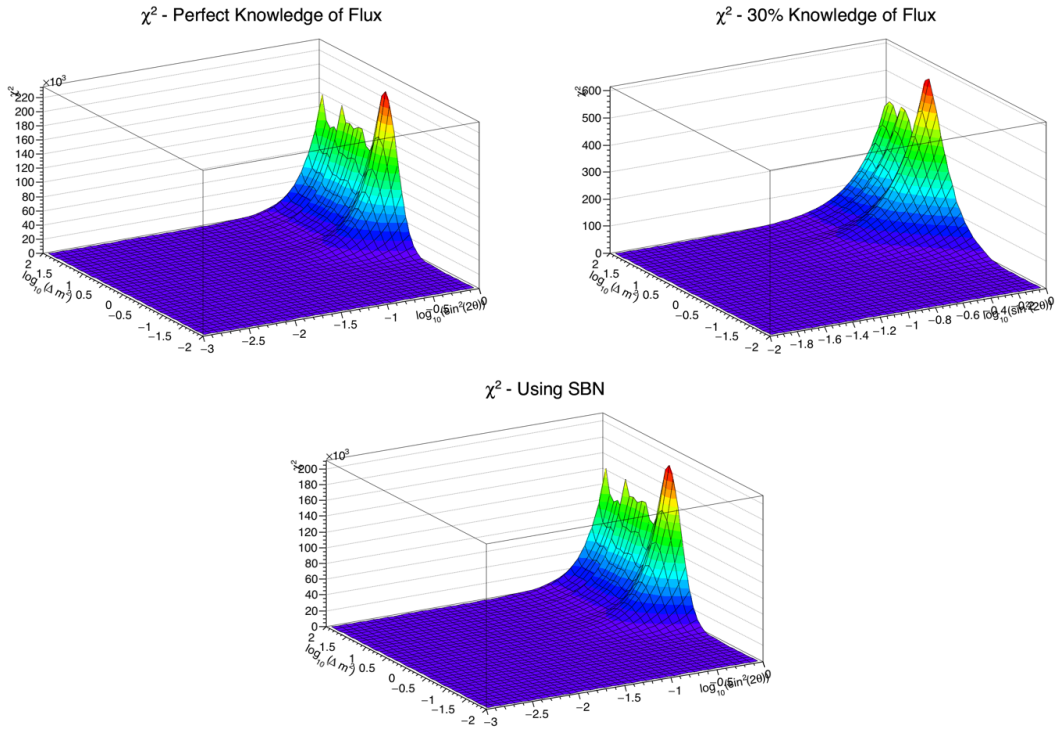

Figure 3: Plots of the χ^2 for different points in the $(\sin^2 2\theta, \Delta m^2)$ phase space for the cases where we have perfect knowledge of the flux (top left), an uncertainty of 30% (top right) and when we add the short baseline detector (bottom). Notice the change of scale in the z-axis, which shows the lost confidence due to the 30% uncertainty and the recovery by adding the near detector.

As with any counting experiment, the statistical error involved in the measurement of N_i is $\Omega_i = \sqrt{N_i}$. The χ^2 statistic can be calculated (in the case of no covariance between the N_i) as

$$\chi^2 = \sum_i \frac{(N_i^{null} - N_i^{osc})^2}{(\Omega_i^{null})^2} = \sum_i N_i^{null} \sin^4(2\theta) \sin^4\left(1.27 \frac{\Delta m^2 \times 0.6}{E_i}\right)$$

This was calculated for different points in the $(\sin^2 2\theta, \Delta m^2)$ phase space. The χ^2s obtained are shown in the top left panel of Figure 3.

Given these, we can identify the 90%, 3σ and 5σ confidence level regions of the phase space as the regions of this space where χ^2 is at least 1.64, 7.75 or 23.40 above its minimum value. These contours are shown in the top left panel of Figure 4.

The region to the right of the contours represents those values of $(\sin^2 2\theta, \Delta m^2)$ that are "ruled-out" by the data. As expected, the 90% CL contour is the left-most one, followed by the 3σ (99.7% CL) and 5σ (0 dot lots of 9s) contours. We now add some constraints to the model.

Computation

A note on the algorithm used to obtain these contours. This was done by following these steps:

1. Build a $(\sin^2 2\theta, \Delta m^2)$ phase space by creating a grid for each variable that's linearly spaced on a log scale, i.e. if g_i represents the elements of a grid of length n with maximum and minimum values M and m,
$$g_i = 10^{m + i(M-m)/(n-1)}$$

2. These two 1d grids define a 2d grid for the phase space. Calculate the χ^2 for each node on this 2d phase space grid: χ^2_{ij}, where $i, j \in \{0, 1, 2, \ldots n-1\}$ (indexing from 0);

3. Find the minimum χ^2 over all points in the grid and calculate the differences $\chi^2_{ij} - \min_{ij} \chi^2_{ij}$;

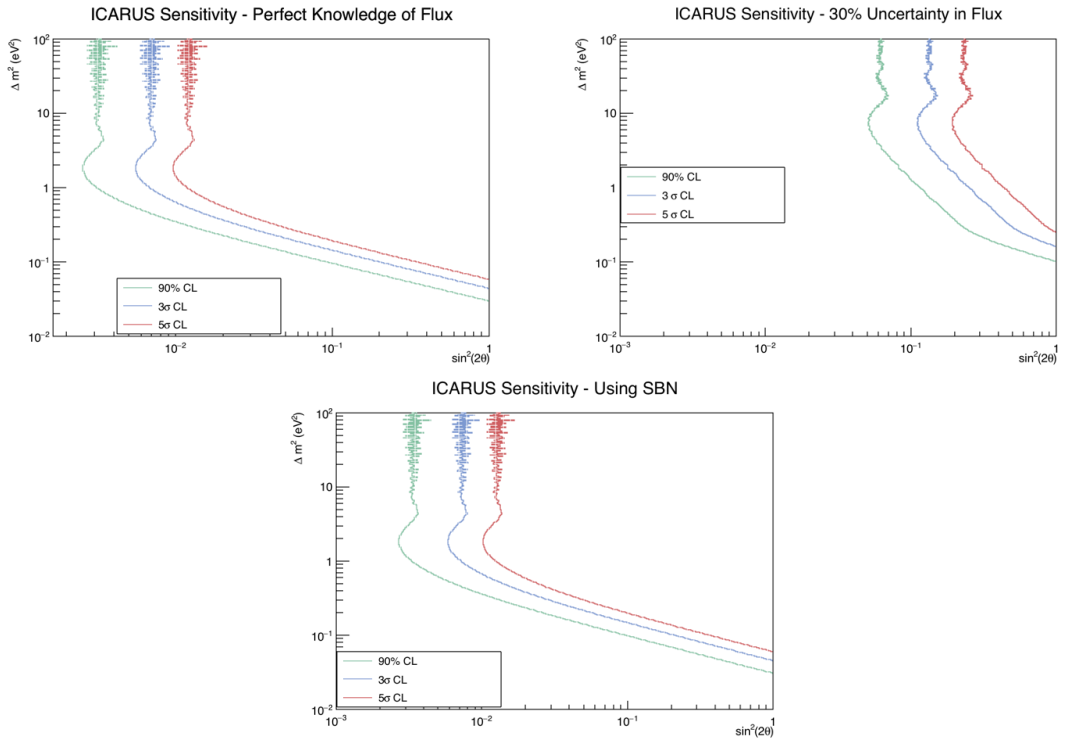

Figure 4: Confidence level contours in the $(\sin^2 2\theta, \Delta m^2)$ phase space for the cases where we have perfect knowledge of the flux (top left), an uncertainty of 30% (top right) and when we add the short baseline detector (bottom). The space to the right of the contours is "ruled-out" from the possible values of $(\sin^2 2\theta, \Delta m^2)$. Notice the change of scale in the x- and y-axes from one plot to another.

4. We now have a 2d grid of size $n \times n$ of χ^2 values relative to their overall minimum. This defines a grid of $(n-1) \times (n-1)$ boxes, each composed of four neighbouring nodes in the 2d grid. As the contour is continuously defined by a specific target $(\chi^2 - \min \chi^2)$ value, we know the contour will pass through the boxes for which this target value lies in between the maximum and the minimum value of the four vertices of each box. We thus assign the midpoint of that box in the $(\sin^2 2\theta, \Delta m^2)$ grid phase space to the points the contour is composed by. This is done for each target $(\chi^2 - \min \chi^2)$ value.

Below is some pseudo-code to elucidate the last step of the above procedure. Assume we are given

- `vector <double> dm2(np), sin(np)`, two vectors of size `np` of doubles for the grids of Δm^2 and $\sin^2 2\theta$, respectively;
- `vector <vector <double> > dchisq(np)`, a vector of size `np` of vectors of size `np` of doubles for the 2d grid of $\chi^2 - \min \chi^2$, where `dchisq[i][j]` corresponds to the point `(sin[i], dm2[j])` of the phase space

The contours are then found using code that resembles this:

```
for each target in {1.64, 7.75, 23.4} {

    * Loop over boxes
    for each i in {0, 1, ... np-1} {
        for each j in {0, 1, ... np-1} {

            * Get vertices
            vertices = {dchisq[i][j], dchisq[i+1][j],
                        dchisq[i][j+1], dchisq[i+1][j+1]}
```

```
                * Find max and min
                min_vertex = minimum of vertices
                max_vertex = maximum of vertices

                * Store midpoint if this box contains the contour
                if (min_vertex <= target <= max_vertex) {
                    store point {0.5*(sin[i+1] + sin[i]),
                                 0.5*(dm2[j+1] + dm2[j])} in a vector
                }

            }
        }

}
```

The following sections were computed via variations of the above methods, usually only changing the computation of the χ^2s.

Imperfect Knowledge of Flux

We now suppose that we only know the flux distribution shown in the left panel of Figure 2 with an uncertainty of 30%. How this affects our analysis is only by increasing the uncertainty in our measurements – adding a systematic error:

$$(\Omega_i^{null})^2 = (\Omega_i^{stat})^2 + (\Omega_i^{sys})^2 = N_i^{null} + (0.3N_i^{null})^2$$

Our χ^2 statistic thus becomes

$$\chi^2 = \sum_i \frac{N_i^{null} \sin^4(2\theta) \sin^4\left(1.27\frac{\Delta m^2 \times 0.6}{E_i}\right)}{1 + 0.9N_i^{null}}$$

This leads to the χ^2s and confidence level contours shown in the top right panels of Figures 3 and 4, respectively. These contours are shifted to the right relative to those described in the previous section, representing a loss of confidence that is expected from adding a new source of (large and systematic) error.

One simplification that was made is that each bin's deviation from the predicted (given initial) flux is independent from the others'. This is not to be expected as it is more likely the predicted flux is off in the same direction and by a similar amount in its predictions of each bins. This dependence would introduce a covariance between bins that would have to be accounted for by estimating the covariance (error) matrix, E_{ij}, and accounting for it in our calculations of the χ^2:

$$\chi^2 = \sum_{i,j} (N_i^{null} - N_i^{osc})(E_{ij})^{-1}(N_j^{null} - N_j^{osc})$$

Assuming the covariance matrix is diagonal (i.e. each bin is independent) simplifies this expression to the one used above.

With Near Detector

One way to counteract this stark loss of confidence in our results is to add another detector nearer to the source. By making a measurement of the flux of neutrinos prior to the same beam reaching the far detector, we exchange our systematic uncertainty in the flux from the source for a (smaller) statistical uncertainty of the same quantity from our measurement at the near detector. Therefore, if the near detector counts a flux described by $N_{near,i}$, our error in the observations at the far detector (which will also go into the χ^2) becomes

$$\Omega_{far,i}^{null} = N_{far,i}^{null} + \left(\sqrt{N_{near,i}^{null}} \frac{N_{far,i}^{null}}{N_{near,i}^{null}}\right)^2$$

where $N^{null}_{far,i}/N^{null}_{near,i}$ is used to rescale the statistical uncertainty $\sqrt{N^{null}_{near,i}}$ for our measurement at the far detector.

As to how these predictions, the N_is, are made, notice that the flux we have (true flux for the null case at 470m) is the original flux coming from the source *minus* that part of it that was detected by the near detector. Thus is we let $\sigma^0_i = \sigma'_i \times 10^{-42}$ be the cross-section of a single argon atom, we have the flux coming from the source

$$\phi^0_i = \phi'_i \times \frac{6 \times 10^{20} \text{ POT}}{10^6} \times (470\text{m})^2 \times \frac{1}{1 - \sigma^0 \times n_{Ar,near}}$$

As such, we have that the flux at the near detector and the counts observed (per energy) is

$$\phi^{null}_{near,i} = \phi^0_i \times \frac{1}{(100 \text{ m})^2}$$
$$N^{null}_{near,i} = \phi^{null}_{near,i} \times (\sigma^0 \times n_{Ar,near})$$

These predictions naturally have an uncertainty involved that includes the 30% uncertainty in the original flux. In predicting the counts at the far detector without priors, this 30% uncertainty would be propagated to that prediction anyway. Assuming, however, that this prediction $N^{null}_{near,i}$ materialises exactly, we can predict the counts at the far detector based on them as such

$$\phi^{null}_{far,i} = \frac{N^{null}_{near,i}}{\sigma^0_i \times n_{Ar,near}} \times (1 - \sigma^0_i n_{Ar,near}) \times \left(\frac{100 \text{ m}}{600 \text{ m}}\right)^2$$
$$N^{null}_{far,i} = \phi^{null}_{far,i} \times (\sigma^0_i \times n_{Ar,far})$$

and this prediction will have an uncertainty as described at the beginning of this section.

As before, $N^{osc}_{far,i} = N^{null}_{far,i} P_{\mu\to\mu}$ so

$$\chi^2 = \sum_i \frac{N^{null}_i \sin^4(2\theta) \sin^4\left(1.27\frac{\Delta m^2 \times 0.6}{E_i}\right)}{1 + N^{null}_{far,i}/N^{null}_{near,i}}$$

This leads to the χ^2s and contours shown in the bottom panel of Figures 3 and 4, respectively. We see that the contours shift back almost to where they were in the base case – the statistical uncertainty from counting error that replaces the 30% systematic uncertainty is very small and reduces our error significantly.

Again, here we make simplification like those described above – each bin shouldn't be completely independent and the covariance matrix should be diagonal.

Imperfect Energy Resolution

If we now assume that our energy resolution in the initial flux is not perfect, Gaussian smearing of the initial spectrum should affect the final contours we obtain – lowering our confidence and pushing them towards the right. We investigate Gaussian smearing of the form $\mathcal{N} \sim (E, f\sqrt{E})$ for $f \in \{0.05, 0.10, 0.25\}$ by applying a convolution using this function to the initial spectrum, i.e. each bin, i, has its counts changed from $N_i \to N'_i = \sum_j \phi_j(E_i)$, where $\phi_j(\cdot)$ is the probability density function for the distribution $\mathcal{N} \sim (E_j, f\sqrt{E_j})$. Figure 5 shows the transformed spectra, with the peak reduced and the tails longer, as expected.

The analysis is then carried out in the same was as described above in the "With Near Detector" section. The resulting 5σ confidence level contours are shown in figure 6. Notice that there's not much of a change between the perfect resolution and the imperfect resolution scenarios (always using the near detector, as in the bottom panel of Figures 3 and 4.

Notice that what we did here is look at the effect of having poor energy resolution in our initial spectrum, which essentially only changes the energy spectrum of the flux coming in to our detectors in the analysis. If we were to look at the effect of a poor energy resolution of the detectors themselves we'd have to convolute those measurements and, again, would have to consider covariances (which we ignored here); bins closer to each other should have a larger covariance since the gaussians centred at each bin has a larger value for neighbouring bins than for faraway ones.

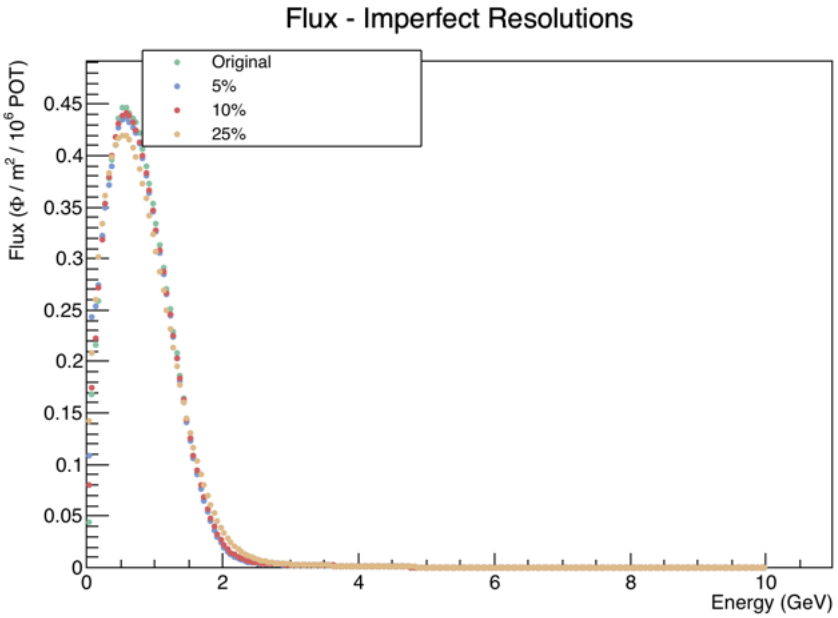

Figure 5: The convoluted flux spectra.

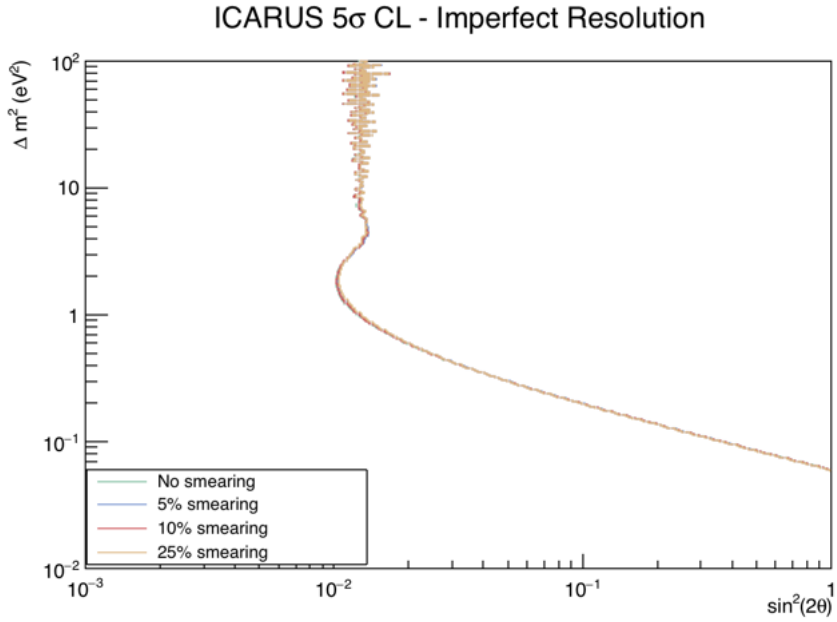

Figure 6: 5σ confidence level contours for varying energy resolutions – there doesn't seem to be much of a change.

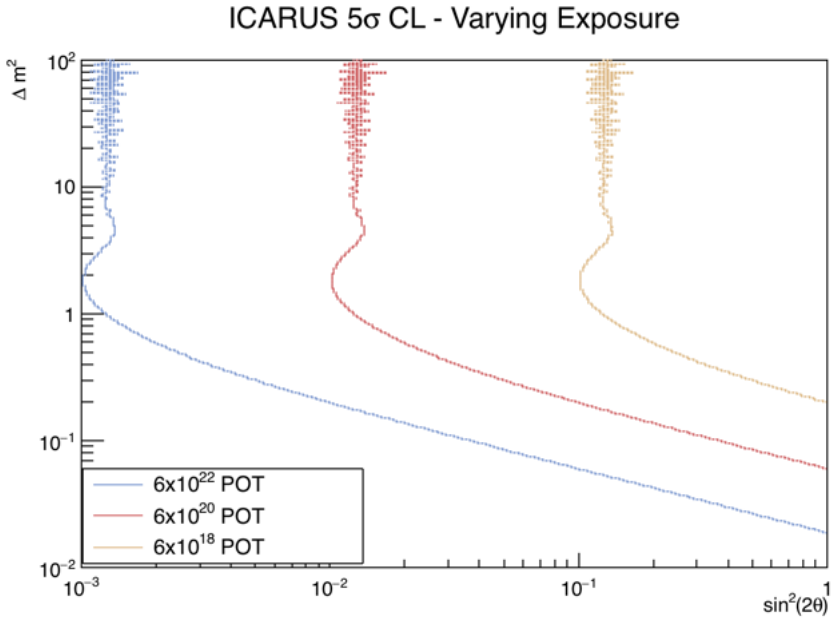

Figure 7: 5σ confidence level contours for varying exposures.

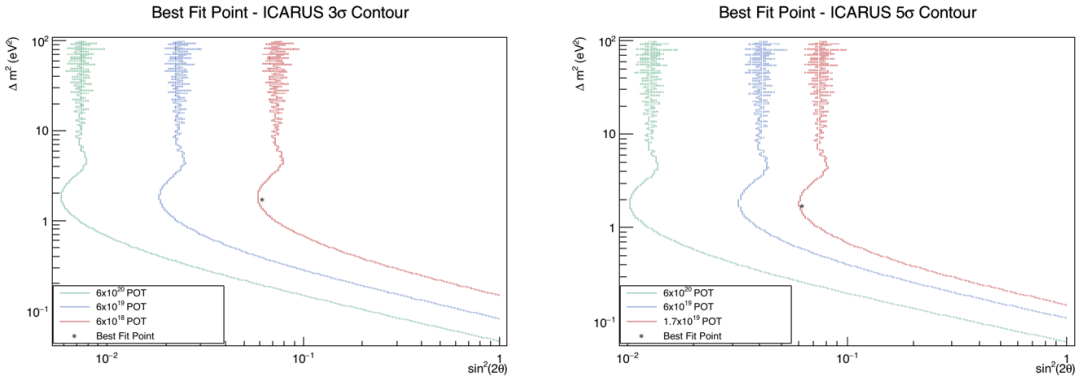

Figure 8: The exposures needed in order to cover the best fit point with the 3σ (left) and 5σ contour (right).

Effect of Exposure

We can also look at the effect of exposure on the sensitivity contours. Figure 7 shows the 5σ contour for exposures 10^{18}, 10^{20} and 10^{22} POT. As expected, more exposure indicated more confidence, pushing the contours towards the right.

We can thus study how adjusting the exposure can allow us to cover the best fit point from past studies with our sensitivity contours. We draw the best fit point from "Updated Global 3+1 Analysis of Short-Baseline Neutrino Oscillations" by Gariazzo et al.:

$$\Delta m^2_{BF} = 1.7 \text{ eV}^2, \ \sin^2(2\theta_{BF}) = 0.062$$

Figure 8 shows the needed exposures in order to cover this point with the 3σ and 5σ contours of our analysis: an exposure of around 6×10^{18} POT for the former and around 1.7×10^{19} POT for the latter.

Further, we can add MicroBooNE into the analysis in the same way we added the near detector in the "With Near Detector" section (though without using it's counts in the errors to account for the uncertainty in the flux) in order to compare the rate of measurement in MicroBooNE and ICARUS. We start MicroBooNE off with 13.2×10^{20} POT (and ICARUS with 0 POT) and examine the volume of observations in both detectors as we add protons on target onto those. Figure 9

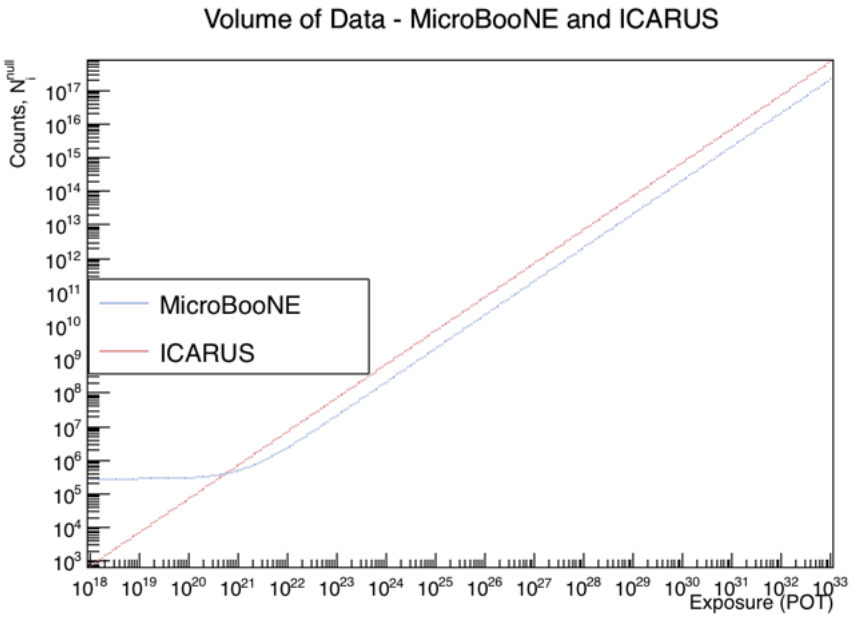

Figure 9: Volume of measurements vs. exposure in each detector.

shows the result. Notice that around 5×10^{20} POT above the initial exposures the volume of observations in ICARUS surpasses that in MicroBooNE due to the larger size of the detector, despite the $1/r^2$ loss in intensity of the beam.

Discussion and Extensions

In all, our analysis suffered from simplification that usually related to the omitting of covariances. This comes in assuming that the errors in different bins are independent from one another – such as when we add an uncertainty in the normalisation of the flux or in the resolution of the detectors – or, additionally, that the errors in the same bin but between different detectors (SBND and ICARUS, in particular) are identical. This second assumption is not necessarily the case; the detectors are different both in terms of geometry and the physics of detection. A more complete analysis would estimate these covariances and dependencies and use them in the unsimplified chi squared

$$\chi^2 = \sum_{ij} (N_i^{null} - N_i^{osc})(E_{ij})^{-1}(N_j^{null} - N_j^{osc})$$

But beyond this, there are various extensions related not to simplifications made in the analysis we carried out but to aspects of the physics of the experiment that were omitted entirely from this analysis. These are better explained with reference to the analysis programme described in the SBND proposal. The document describes a systematic error matrix that is the (linear) combination of a series of independent major sources of error. These are uncertainties regarding the flux, the neutrino reaction cross-sections, the cosmic background, dirt events (events that may happen anywhere other than in the liquid argon of the detectors, e.g. the ground in between detectors, different parts of the detector itself, etc.), and the functioning of the detectors:

$$E^{\text{syst}} = E^{\text{flux}} + E^{\text{x-sec}} + E^{\text{cosmic}} + E^{\text{dirt}} + E^{\text{detector}}$$

Within each of these general categories of independent systematic uncertainties, covariances will exit and must also be accounted for. In a complete analysis of the sensitivity of our experiment, all of these uncertainties will have to be estimated and considered.